Journal of Photochemistry & Photobiology, B: Biology 183 (2018) 64–74

Contents lists available at ScienceDirect

Journal of Photochemistry & Photobiology, B: Biology

journal homepage: www.elsevier.com/locate/jphotobiol

Solution-combustion synthesis of doped TiO_2 compounds and its potential antileishmanial activity mediated by photodynamic therapy

A.A. Lopera[a,b], A.M.A. Velásquez[b,c], L.C. Clementino[b,c], S. Robledo[d], A. Montoya[d], L.M. de Freitas[b], V.D.N. Bezzon[e], C.R. Fontana[b], C. Garcia[a,*], M.A.S. Graminha[b]

[a] Universidad Nacional de Colombia, Sede Medellín, Grupo de Cerámicos y Vítreos, Colombia
[b] School of Pharmaceutical Sciences, São Paulo State University (UNESP), Araraquara, Brazil
[c] São Paulo State University (UNESP), Institute of Chemistry, Araraquara, Brazil
[d] Universidad de Antioquia, PECET-Instituto de Investigaciones Médicas, Facultad de Medicina, Colombia
[e] Department of Pharmacy, Faculty of Pharmaceuticals Science, University of Sao Paulo, Brazil

ARTICLE INFO

Keywords:
Pt-doped TiO_2
Zn-doped TiO_2
Photodynamic therapy
Nanostructures
Leishmanicidal activity

ABSTRACT

Photodynamic therapy has emerged as an alternative treatment for cutaneous leishmaniasis, and compounds with photocatalytic behavior are promising candidates to develop new therapeutic strategies for the treatment of this parasitic disease. Titanium dioxide TiO_2 is a semiconductor ceramic material that shows excellent photocatalytic and antimicrobial activity under Ultraviolet irradiation. Due to the harmful effects of UV radiation, many efforts have been made in order to enhance both photocatalytic and antimicrobial properties of TiO_2 in the visible region of the spectrum by doping or through modifications in the route of synthesis. Herein, Fe-, Zn-, or Pt- doped TiO_2 nanostructures were synthesized by solution-combustion route. The obtained compounds presented aggregates of 100 nm, formed by particles smaller than 20 nm. Doping compounds shift the absorption spectrum towards the visible region, allowing production of reactive oxygen species in the presence of oxygen and molecular water when the system is irradiated in the visible spectrum. The Pt (EC_{50} = 18.2 ± 0.8 μg/mL) and Zn (EC_{50} = 16.4 ± 0.3 μg/mL) –doped TiO_2 presented the higher antileishmanial activities under visible irradiation and their application as photosensitizers in photodynamic therapy (PDT) strategies for the treatment of cutaneous leishmaniasis should be considered.

1. Introduction

Leishmaniasis is a neglected disease caused by parasites from the genus *Leishmania*. This parasitic disease is endemic in 98 countries and > 90% of new cases occur in Brazil, Ethiopia, India, Somalia, South Sudan, and Sudan according to the World Health Organization [1]. The cutaneous form of the disease is the most common manifestation, presenting an annual incidence of 0.7 to 1.3 million new cases [2,3]. The available therapeutic drugs for leishmaniasis treatment are still based on pentavalent antimonials, amphotericin B, miltefosine or paromomycin, which present several limitations such as toxicity, difficult route of administration and variable efficacy [4], and although many efforts have been made towards the discovery of new synthetic or natural antileishmanials [5–12], new therapeutic options are still needed. In recent years, photodynamic therapy (PDT) has been investigated as a potential alternative to control cutaneous leishmaniasis (CL) [13–16]. PDT consists in administration of a photosensitizer at the site of wound activated by light at appropriate wavelength, culminating in the production of microbicidal reactive oxygen species (ROS) [17]. Although several organic photosensitizers was evaluated in CL treatment [13,15,18–22], they showed different drawbacks such as photobleaching or low stability under irradiation. In order to circumvent these problems, inorganic-based compounds have been investigated as alternative photosensitizers for PDT, including silver (Ag), gold (Au), zinc (Zn), magnesium oxide (MgO), and titanium dioxide (TiO_2), showing reduced photo bleaching effect, increased singlet oxygen quantum yield and thermal/photochemical stability as well as facilitated immobilization onto substrates [23,24].

TiO_2 is a highly abundant ceramic material that presents anatase, brookite and rutile as its crystalline polymorphic forms and its chemical stability and low toxicity make it suitable for several technological/biotechnological applications including its use in pigment and cosmetic industries, as well as in biomedical sectors [25–29]. On the other hand, TiO_2 nanostructures are only excited by light in the ultraviolet (UV) region of the electromagnetic spectrum [30], which compromises its photoactivity-based biomedical uses due to UV light deleterious effects,

* Corresponding author.
E-mail address: cpgarcia@unal.edu.co (C. Garcia).

https://doi.org/10.1016/j.jphotobiol.2018.04.017
Received 17 November 2017; Received in revised form 6 April 2018; Accepted 11 April 2018
Available online 13 April 2018

such as mutation induction. Besides, longer wavelengths (as visible light, in comparison to UV) would have a better penetration performance to reach the tissues where infected cutaneous macrophages reside, and thus activate the photosensitizers at the place where they should act. We have recently shown the synthesis by self-combustion route of Pt-doped TiO_2 compounds that absorb light in the visible region, and their application in pollutants degradation [31,32], however, their photodynamic activity has yet to be explored. The potential of metal-doped TiO_2 compounds for acting as photosensitizers can be exemplified by TiO_2-Ag nanoparticles obtained by hydrothermal route, which under visible light, alone or in combination with other antileishmanial agents, have shown in vitro leishmanicidal effect [25,27,28]. Herein, we report the synthesis, structural and morphological characterization of Zn-, Fe_2O_3- and Pt- doped TiO_2 based nanoparticles [33] using solution-combustion synthesis method. Their cytotoxicity and antileishmanial activity under photoactivation in the visible region were also evaluated in vitro against murine macrophages and *L. amazonensis* amastigote forms, respectively.

2. Experimental Procedure

2.1. Synthesis of Zn, Fe, and Pt doped TiO_2 Based Compounds

Doped TiO_2 compounds were synthesized as previously described [31]. Briefly, Titanium (IV) isopropoxide ($Ti[OCH(CH_3)_2]_4$; Alfa Aesar - Heysham, Lancashire, UK), Zinc nitrate hexahydrate ($Zn(NO_3)_2 6H_2O$; Sigma-Aldrich Co. LLC - St. Louis, MO, USA), Iron nitrate nonahydrate ($Fe(NO_3)_3\ 9H_2O$; Merck - Kenilworth, NJ, USA), Platinum tetrachloride ($PtCl_4$, Sigma-Aldrich Co. LLC - St. Louis, MO, USA), and Glycine ($C_2H_5O_2N$; Alfa Aesar - Heysham, Lancashire, UK) were used as reagents. The titanyl nitrate is prepared by dissolving titanyl hydroxide, $TiO_2(OH)$ in diluted acid nitric. The appropriate amount of Ti (IV) isopropoxide was mixed with 25 mL of distilled water for each doped TiO_2 compound under vigorous stirring at 0 °C for one hour in order to obtain Titanyl hydroxide. Then, Titanyl hydroxide was mixed with nitric acid to obtain Titanyl nitrate. After obtaining Titanyl nitrate, the doping metal was added in a molar relation of 0.6%. Subsequently, glycine was added to the above solution under stirring for additional 5 min. Fuel-oxidizer mixture was brought to room temperature and placed on a hot plate at 90 °C in order to slowly remove the water until a white resin was formed. The resin was further heated to 180 °C increasing the heating of the plate and monitoring it by a thermocouple. This heating produced an exothermic reaction in two stages, and the recovered powder was carried to grinding in a Retsch alumina ball mill PM 100 for further characterization.

2.2. Structural and Morphological Characterization of Zn-, Fe- and Pt-doped TiO_2

The powders obtained were evaluated using a X-ray powder "diffractometer model RINT2000 from Rigaku (Tokyo, Japan) with bragg-brentano geometry, $CuK\alpha_{1/2}$ radiation, operating in reflection mode. The data were collected using a position sensitive detector in a diffraction range of 20–80° (2θ)". Refinements were performed through Rietveld method [34] using GSAS software [35] for the samples studied in this work. It was quantified the weight proportion of the phases in each sample as well as their crystallite size. Morphology and microstructure were analyzed using scanning electron microscopy and scanning electron microscopy – energy dispersive spectroscopy (SEM-EDS) (SEM; Carl Zeiss - Oberkochen, Germany), field emission SEM (FE-SEM, JEOL JSM-field - 6701F - Peabody, MA, USA) and transmission electron microscopy, TEM (TEM-CM100, Philips - Amsterdam, Netherlands).

2.3. Preparation of Zn-, Fe- and Pt- doped TiO_2 Dispersions for Biological Analysis

Zn-, Fe- and Pt-doped TiO_2 powders were sterilized in an autoclave at 120 °C for 20 min. Stock solutions were adjusted to 20 mg/mL in 1 × Phosphate Buffered Saline (PBS Buffer, 137 mM NaCl; 2.7 mM KCl; 10 mM Na_2HPO_4; 1.8 mM KH_2PO_4) followed by sonication for 30 min.

2.4. UV-VIS Characterization and ROS Measurement

Optical properties of powders before or after heat treatment were analyzed by diffuse reflectance spectroscopy and UV-VIS absorption using a PerkinElmer spectrophotometer (Lambda 950 UV/Vis, PerkinElmer - Waltham, MA, USA) with 280–800 nm spectral range.

A white LED light source (LED lamp) was used for photodynamic activation. The LED lamp emission spectrum was characterized by UV-VIS spectrophotometry (USB2000, Ocean optics, Largo, FL, USA) and its output power was measured (PM100D, Thorlabs Inc., Newton, NJ, USA). Indirect detection of ROS was performed using a stock solution (2 mM) of H_2DCF-DA (2′,7′ dichlorofluorescein diacetate – Sigma–Aldrich®) freshly prepared in Dimethyl sulfoxide (DMSO). For this, 20 μg/mL of Zn-, Fe- and Pt-doped TiO_2 compounds were suspended in 200 μL of PBS in the presence of H_2DCFDA (10 μM). Immediately, the system was subjected to white LED irradiation and monitored for 60 min. Fluorescence was measured spectrofluorometrically at 520 nm using an excitation wavelength of 488 nm (Synergy H1 Multi-Mode Reader, BioTek Winooski, VT, USA) Tecan Infinite® 200 pro. Assays were carried out in triplicate.

2.5. Parasite Culture

Promastigotes of *L. amazonensis* MPRO/BR/1972/M1841-LV-79 were maintained at 28 °C in liver-infusion tryptose medium (LIT) supplemented with 10% heat-inactivated fetal bovine serum (FBS). Promastigote form cultures were carried out until exponential growth phase (1×10^7 parasites/mL).

2.6. Evaluation of Cytotoxicity on Murine Macrophages

Peritoneal macrophages were obtained as previously reported [36]. In brief, cells were collected from adult male Swiss albino mice peritoneal (6 to 8 weeks old and 25–30 g weight) previously stimulated with thioglycolate and seeded into 96-well plates at a density of 5×10^6 macrophages/mL (100 μL/well) in RPMI 1640 medium supplemented with 10% heat-inactivated FBS, 25 mM HEPES, 2 mM L-glutamine, 1% penicilin/streptomycin (Sigma-Aldrich) and incubated for 4 h at 37 °C in a 5% CO_2-air mixture for cell adhesion. Then, supernatants were removed and fresh media containing different concentrations of TiO_2 compounds ranging from 1 to 300 μg/mL were added; the plates were incubated for 4 h followed by irradiation with visible light (22 mW/cm^2; 52.8 J/cm^2) for 40 min. After light exposure, cells were incubated under the same conditions for 24 h and their viability was measured by the MTT colorimetric assay [5]. As a control, the same procedure was used but the plates were placed under dark conditions during the whole incubation. Absorbance was read on a spectrophotometer (Tecan Infinite® 200 pro) at 540 nm. Cytotoxic concentration of compounds that resulted in 50% of cell growth inhibition (CC_{50}) was determined.

2.7. Evaluation of In Vitro Antiamastigote Activity

To evaluate the antileishmanial activity of Zn-, Fe- and Pt-doped TiO_2 compounds on intracellular *L. amazonensis* amastigotes, we used a method previously described with some modifications [36]. Murine

peritoneal macrophages in RPMI 1640 supplemented with 10% heat-inactivated FBS were seeded at a density of 1×10^5 cells/well on coverslips of 13 mm diameter arranged in a 24-well plate. Promastigote forms of *L. amazonensis* at stationary growth phase were added to the wells in a ratio of 5:1 (promastigotes: macrophages) after 4 h of incubation at 37 °C and 5% CO_2- air mixture to allow the adhesion of macrophages, and incubated for 4 h to allow parasites internalization, followed by wash with PBS 1× to remove the non-internalized parasites. Infected macrophages were further incubated in RPMI 1640 medium for 24 h at 37 °C in 5% CO_2-air mixture to allow parasite differentiation to amastigotes as well as parasite multiplication. Macrophages containing amastigotes were then treated with TiO_2 compounds ranging from 1 to 25 μg/mL for 4 h prior to light irradiation. For irradiation, cells were exposed to the light source for 40 min (22 mW/cm^2; 52.8 J/cm^2), followed by incubation for 24 h at 37 °C and 5% CO_2-air mixture. The same procedure was used as control but the plates were placed under dark conditions during the whole incubation time. For parasite quantification, cells were fixed with methanol, stained with Giemsa and examined under a light microscope (Zeiss Opton – Carl Zeiss, Oberkochen, Germany) at 100× magnification. The concentration that resulted in a 50% decrease in parasite number was determined by regression analysis and expressed as EC_{50}. All the experiments were carried out in triplicate. Cytotoxicity for host cells and parasites were compared and expressed as selectivity index (SI), which was defined as the ratio between CC_{50} and EC_{50}.

2.8. Uptake of Nanoparticles (NPs) Charged With Fluorescent Compound in huMDM

Since TiO_2 compounds do not exhibit significant fluorescence, nanoparticles were loaded with hypericin, a natural-occurring molecule that emits red fluorescence (600–680 nm) when excited by green light (540–580 nm). The methodology used was the agitation-impregnation technique. 20 mg of particles were re-suspended in a hypericin stock solution at 10uM and strongly agitated during 72 h in dark conditions. After this time, particles were centrifuged and washed to remove adsorbed or not adsorbed hypericin on the compounds. In order to evaluate if nanoparticles uptake can be made by human cells, monocyte-derived human macrophages (huMDMs), obtained as previously described, were used [37]. The huMDMs were cultivated in the presence of 20 μg/mL of NPs loaded with hypericin. After 2 and 4 h of incubation, cells were washed with PBS to remove non-interiorized particles and to be analyzed under a fluorescence microscope (Nikon Labophot-2 – Nikon, Minato, Tokyo, Japan). Cell uptake capacity of NPs was determined based on fluorescence intensity measurement. It was possible to detect qualitatively the distribution of the compounds in the cells by optical microscopy.

2.9. Ethics Statement

Animal experiments were approved by the Ethics Committee for Animal Experimentation of Sao Paulo State University (UNESP), School of Pharmaceutical Sciences (CEUA/FCF/CAr: 43/2016), in agreement with the guidelines of the Sociedade Brasileira de Ciência de Animais de Laboratório (SBCAL) and of the Conselho Nacional de Controle de Experimentação Animal (CONCEA).

2.10. Statistical Analysis

Statistical analyzes were carried out using GraphPad InStat software (GraphPad Software, Inc. - La Jolla, CA, USA). Statistical differences between groups were evaluated using one-way analysis of variance [38], followed by the Student-Newman-Keuls multiple-comparison test and considered significant when P values were ≤ 0.05.

3. Results and Discussion

3.1. Structural Characterization

The diffractograms of TiO_2 powders obtained by combustion in

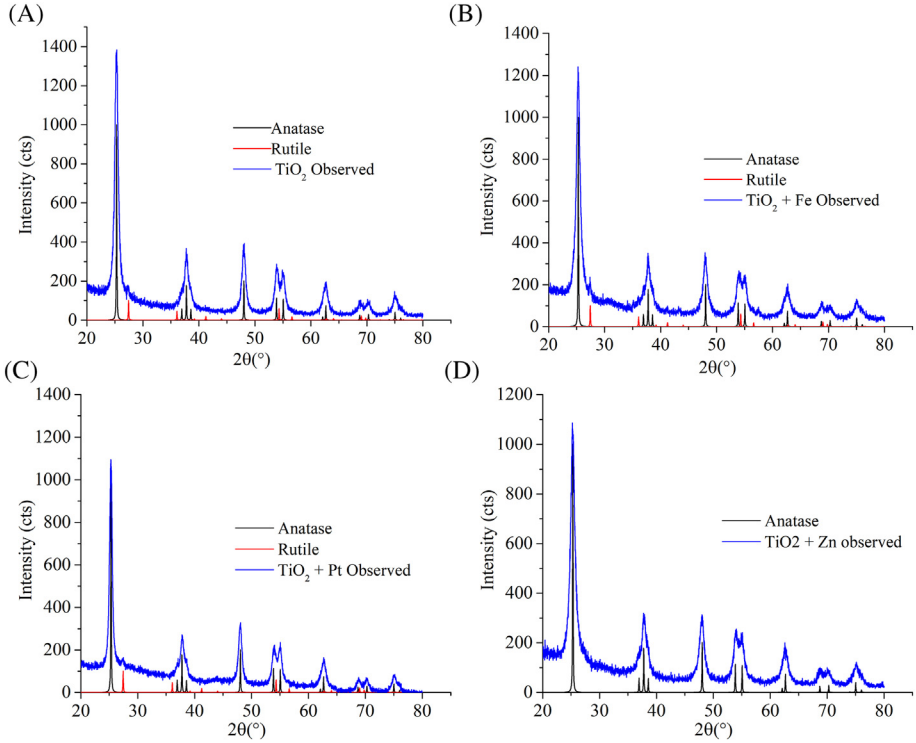

Fig. 1. X-ray diffractograms of TiO_2 powders obtained by combustion in solution. A) TiO_2; B) TiO_2 with Iron (TiO_2 + Fe); C) TiO_2 with platinum (TiO_2 + Pt); D) TiO_2 with Zinc (TiO_2 + Zn).

Table 1
Quantification of anatase or rutile phase and crystallite size obtained by Rietveld refinement of TiO_2 -doped compounds.

Compound	Anatase (% wt)	Rutile(% wt)	Crystallite size (anatase) (nm)
TiO_2	93.98	6.01	12.394
TiO_2 + Zn	100	–	9.285
TiO_2 + Fe	94.84	5.15	10.98
TiO_2 + Pt	92.122	7.877	11.44

solution are shown in Fig. 1 (A–D). It is important to note the peak broadening is related to the nanocrystalline nature of the samples. The phases identified are in accordance with Joint Committee on Powder Diffraction Standards (JCPDS) cards No. 21-1272 and No. 76-1940 for anatase and rutile phases, respectively. The simulations presented in Fig. 1 were performed by Mercury software V 3.9 [39] using the crystallographic information file (crystal structure) obtained at the Inorganic Crystal Structure Database (Cambridge Structural Database CSD) [40] under the codes 9161 (rutile) and 9852 (anatase), and as can be seen the peaks observed agreed with the simulated ones. Refinements were performed using the above mentioned ICSD structures; the phase quantification are shown in Table 1. In all synthesis except the one that used Zn as precursor, the amount of rutile was determined (Rietveld analysis) as being < 10% in weight. It is possible to observe that the crystallite size changes when dopants are present. With Fe, Pt, and Zn doping can be done by substitution. With Pt, Pt^{4+} and Pt^{2+} can replace Ti^{4+} [41]. With Zn it is possible the substitution of Zn^{2+} by Ti^{4+} [42] and in case of Fe, Fe^{+3} can be introduced into the sublattice of TiO_2 [43]. Doping can produce lattice distortion, crystallinity decrease and decrease in the crystallite size (Table 1) [44,45] [46]. Doping can also induce the formation of oxygen vacancies in order to maintain the neutrality of the structure load [47].

The Fig. 2 shows the Raman spectra of the samples showing the peaks associated to anatase phase at 144 cm^{-1}, 197 cm^{-1}, 399 cm^{-1}, 519 cm^{-1} and 641 cm^{-1}, which correspond to Eg, B1g, A1g (superimposed with B1g), and Eg modes of anatase phase. Mode A1g is representing the pure O vibration, B1g mode is the pure Ti vibration, and Eg mode belongs to the vibration of mix of O-atom and Ti-atom motions [48]. The SEM analyses depicted in Fig. 3 show that Zn-, Fe- and Pt-doped TiO_2 powders present aggregates below 10 μm (Fig. 3A, B, C, D; left) and particles below 100 nm (Fig. 3A, B, C, D; right). SEM-EDS spectra confirm the presence of Zn and Fe as dopants (Fig. 4A and B, respectively), but not Pt (Fig. 4C), which is probably due to the peak associated with Au used for coating (Au ~ 2.1 eV) causing overlap with the peak associated with Pt. TEM images confirmed that all samples are composed of granular aggregates smaller than 20 nm (Fig. 5), demonstrating that the synthesis by combustion route allows the obtention of nanocrystalline powders. It is well known that combustion synthesis is a process that involve simultaneous oxidation and reduction process between oxidant and reducer or fuel. The nitrates salts are excellent oxidants for the combustion synthesis due to its solubility and possibility to form complex with the fuel. Herein, TiO_2 compounds was obtained using glycine as fuel and titanyl nitrate, as oxidant. Glycine acts as complex agent and reducer during the synthesis. When the reaction reaches the ignition temperature, an exothermic reaction occurs leading to temperatures above 1500 °C, which are sufficient to form the desired phases without further thermal treatment [49], such as the anatase, the main phase herein obtained. Moreover, morphology, particle size and surface area of these aggregates might be correlated to the low amount of gases released during the combustion [31] [49,50].

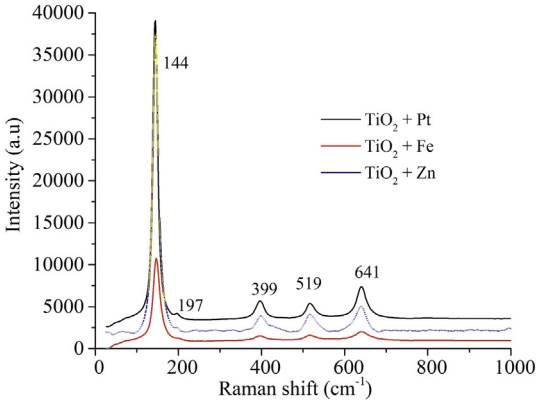

Fig. 2. The Raman spectra of the TiO_2-doped compounds.

3.2. Characterization of the Light Source

Fig. 6 shows the spectrum of emission of the LED light source used to irradiate the TiO_2 compounds. The LED light presented only emission at 450 nm and 552 nm.

3.3. UV–Vis Absorption Studies and Measurement of ROS Generation by TiO_2 Compounds Upon Visible Irradiation

Fig. 7A shows the UV–vis spectrum of non- doped and doped TiO_2 samples. The absorption intensity was shifted to the visible light range (low energy) for TiO_2 -doped compounds when compared to non -doped TiO_2 or commercial TiO_2. Similar observation was also shown for carbon, iron, zinc or platinum doped -TiO_2 compounds, inducing a shift in the absorption spectra to the red [51,52]. The band gap energy for TiO_2 samples was estimated from the Tauc relationship $\alpha h\nu = A(h\nu - E_g)^n$ [53] where α is the absorption coefficient which is proportional to the function of the reflectance (F(R)) according with the Kubelka – Munk model, $h\nu$ is the photon energy, A is a proportional constant, E_g is the band gap energy and n is a factor dependent of the transition nature which is 2 for TiO_2 in the anatase phase [54]. In Fig. 7B, the band gap energies are 1.88 eV, 2.50 eV, 3.01 eV, 3.11 eV, and 3.25 eV for Fe-, Zn-, Pt- doped TiO_2, non –doped TiO_2 and commercial TiO_2, respectively. The optical absorption threshold wavelength (λg) was calculated using the equation λg = 1240/Eg, The samples exhibited a red shift to the visible light ranging from 411 nm to 688 nm when compared to the non-doped TiO_2 (398 nm), which demonstrates that the doped TiO_2 might be improving the absorption of the visible light. The photocatalytic activity was examined through the ROS production. Fig. 8 shows that Fe- doped TiO_2 presented the lowest production of ROS, even lower than commercial anatase, regardless its higher capacity of light absorption in the visible region when compared to other compounds. Similarly, Özge Kerkez-Kuyumcu et al. [51] attributed the lower activity of Fe by their inability to act as intermediate energy levels to hold electrons leaping from valence band of TiO_2. The interaction of titania loaded and Fe metal ions might have created a number of surface defects, which increased the probability of recombination of the light induced charges. It is known the visible light catalytic respond for a doped semiconductor could be attributed to the three incentives: (1) Impurity levels associated to dopant into the TiO_2 lattice, (2) Oxygen vacancy induced by the dopant due charges differences, (3) Secundaries phases of dopant associated with the catalyst surface [46]. In the first case the presence of dopants can generate intermediate states of energy in the TiO_2 gap below the conduction band and fulfill functions as trapping centers. These states can involve the excitation of the *3d* electrons of the dopant ion to TiO_2 conduction band according to their respective energy level. In the second case the dopants Fe, Zn, Pt have different valence states than Ti^{4+} and, as a consequence, may have induced the generation of oxygen vacancies during synthesis. Oxygen vacancies influence the photocatalytic response of the material due to the direct alteration of the surface charge and the oxidation potential of the valence band [47] [43]. It is important to note that it has been found that synthesis by combustion in solution can

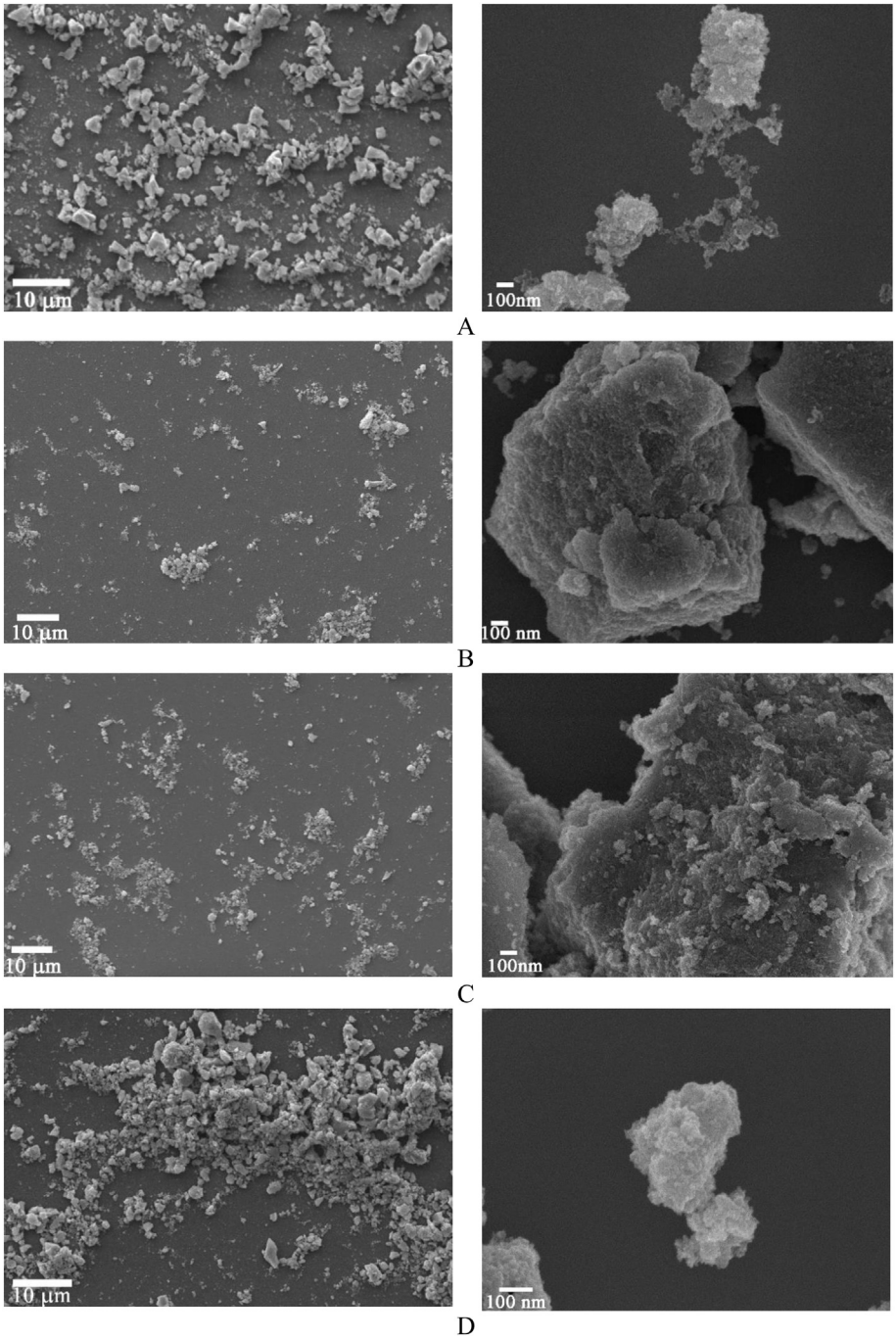

Fig. 3. SEM micrographs of TiO_2 NPs and TiO_2 -doped powders A) TiO_2 + Fe B) TiO_2 + Zn C) TiO_2 + Pt D) TiO_2.

generate doping with carbon atoms and nitrogen as a product of the reaction reducing atmosphere produced during the synthesis [55]. In the three case it is possible to find the dopant as a secondary phase associated with the surface of TiO_2 i.e. PtO, Fe_2O_3 and ZnO which can also affect the photocatalytic response [56].

Fig. 9 shows a scheme of photocatalytic reaction mechanisms of H_2DCFDA oxidation over doped-TiO_2 under visible light irradiation when only the effect of intermediate levels of energy associated with the dopant is considered. When VIS light irradiated the TiO_2 doped photo-induced electrons were excited from the impurity level to the conduction band of TiO_2 and remained h^+ in the impurity level. Then Electrons in the conduction band of TiO_2 could react with adsorbed O_2, generating ·O2, ·H_2O_2 and ·OH radicals via one-step or multistep reactions. Residual holes in the impurity could react with adsorbed water to produce ·OH. These ROS species degrade the H_2DCFDA molecule to its fluorescent form (DCF) increasing the species ROS and thus the fluorescence intensity.

3.4. Uptake of Nanoparticles by Human Macrophages (huMDM)

Fluorescence microscopy analysis (Fig. 10) suggests that huMDM cells were able to uptake NPs. In Fig. 10A, a photomicrograph of TiO_2 aggregate conjugated with hypericin, exhibits orange-reddish fluorescence, indicating that the fluorescent marker was successfully conjugated to the particle surface. Fig. 10B and C show photomicrographs of huMDM cells incubated with TiO_2 compounds for 2 and 4 h. At 2 h the cell shows green fluorescence and at 4 h the cell shows orange-

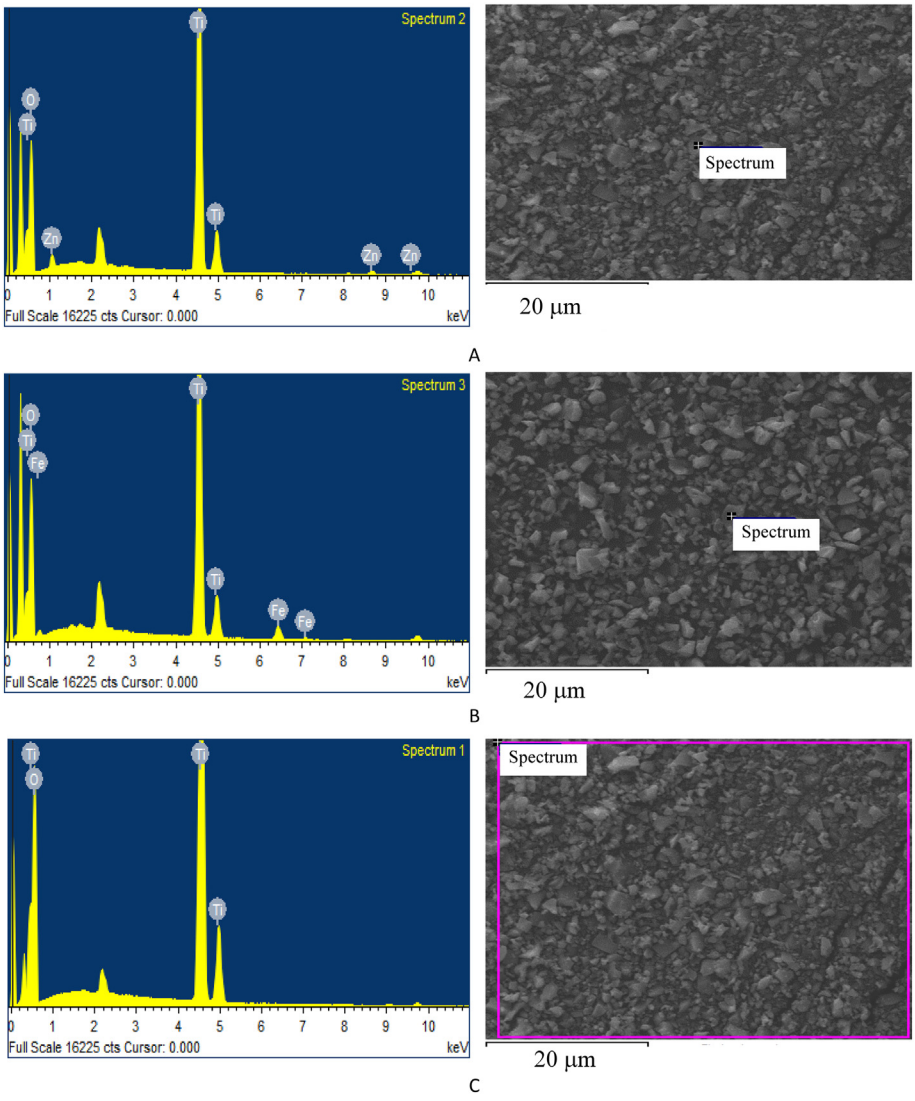

Fig. 4. SEM microscopy micrographs of TiO_2 NPs and TiO_2 doped powders.

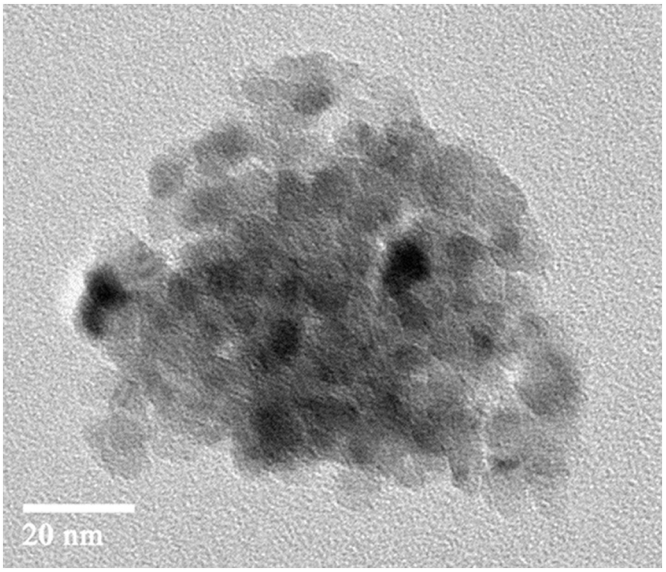

Fig. 5. Transmission electron microscopy (TEM) image of TiO_2 compounds.

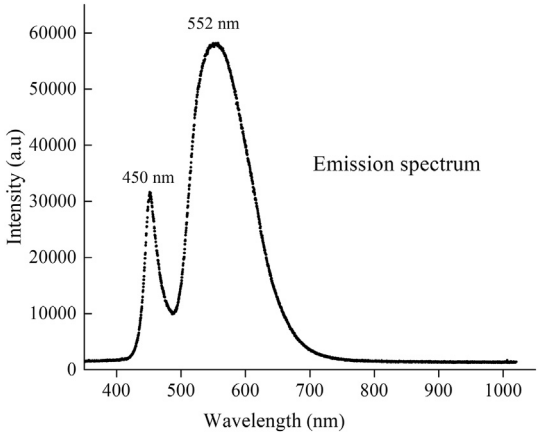

Fig. 6. Emission spectrum of the visible light source used in different assays. The output power measured was of 22.6 mW/cm^2 in a distance of 15 cm.

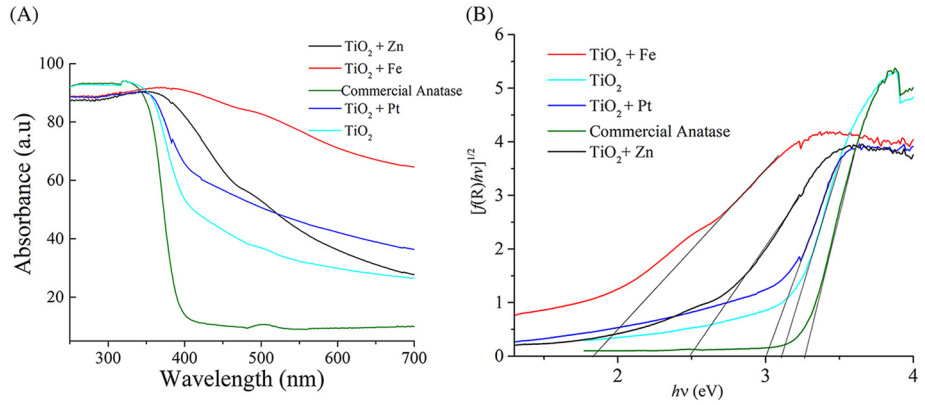

Fig. 7. A. Absorption spectra of TiO_2 NPs and TiO_2 NPs doped with iron (Fe), zinc (Zn), and platinum (Pt). A spectrum of commercial TiO_2 in anatase phase was added for comparison. B. Calculation of Band gap energy (eV).

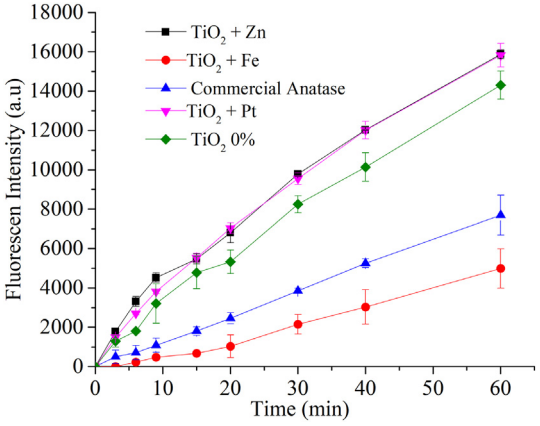

Fig. 8. Fluorescence intensity vs time indicating ROS production of TiO_2 NPs and TiO_2 doped with Iron (Fe), Zinc (Zn) and Platinum (Pt).

reddish fluorescence indicating that as more time, the cells were able to uptake more particles. Fig. 11 shows optical microscopy photographs of macrophages incubated at different concentrations of TiO_2 NPs (20 μg/mL–50 μg/mL). A–D corresponds to control group (without the presence of NPs) and C–D correspond to macrophages with NPs incubated for two hours. After two hours of incubation, it was possible to observe black spots associated with TiO_2 compound which tend to form aggregates when concentration increases. It is also possible to observe NPs inside or surrounding the cell membrane. Although there is no standard methodology for measure the levels of nanoparticles cells uptake, the observed fluorescence inside the cells might be correlated to nanoparticles uptake, i.e., the more the uptake, the higher the fluorescent intensity, which can be depicted in Figs. 10A and B (right) [57,58]. It is worth to note that the relationship between physical properties and levels of uptake of NPs by cells have not been fully clarified [59]. It is reasonable to infer that the amount of particles inside the cell is related to its size, i.e., large particles might enter the cells by active mechanisms such as phagocytosis or endocytosis, whilst small particles, through diffusion events [38,60] or some particles may remain associated with cell membrane and do not penetrate it [59].

3.5. Evaluation of In Vitro Activity of NPs Against L. amazonensis intracellular amastigote forms and their parasite selectivity

The photo-activated compounds Pt- (EC_{50} = 18.2 ± 0.8 μg/mL; SI = 3.2) and Zn- (EC_{50} = 16.4 ± 0.3 μg/mL; SI = 1.9) doped TiO_2 presented antileishmanial activity against *L. amazonensis* intracellular amastigotes (Fig. 12A; Table 2), which might be correlated to ROS production (Fig. 8). TiO_2 doped with Fe or TiO_2 without doping did not present antileishmanial activity at 25 μg/mL, being this value the maximum concentration tested (Fig. 12A). The observed antiparasitic activity for compounds doped with Pt and Zn might be related to their ROS production capacity (TiO_2 + Pt ≅ TiO_2 + Zn > TiO_2 > TiO_2 + Fe), (Fig. 8) and the variation in tolerance and susceptibility due to oxidative stress that leishmania parasites could have. Other factors such as particle size and shape, and specific area at nano scale play an important role in potential

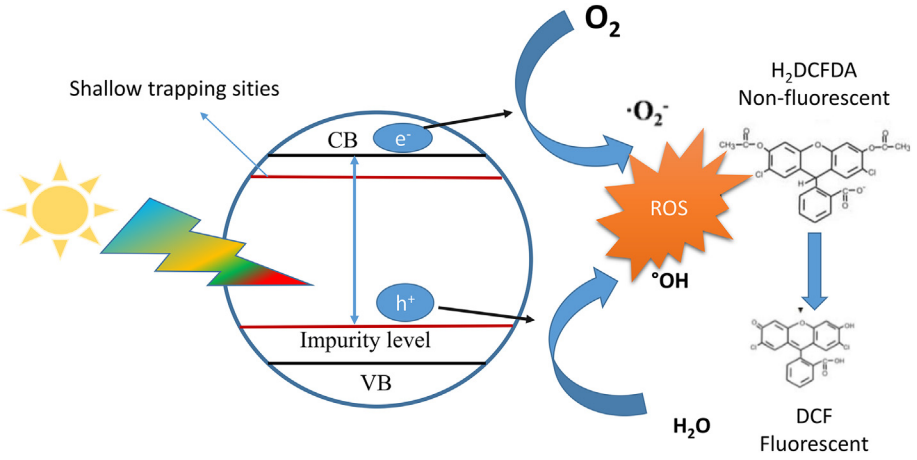

Fig. 9. Scheme of the photocatalytic reaction mechanisms of H_2DCFDA oxidation over doped-TiO_2 under visible light irradiation.

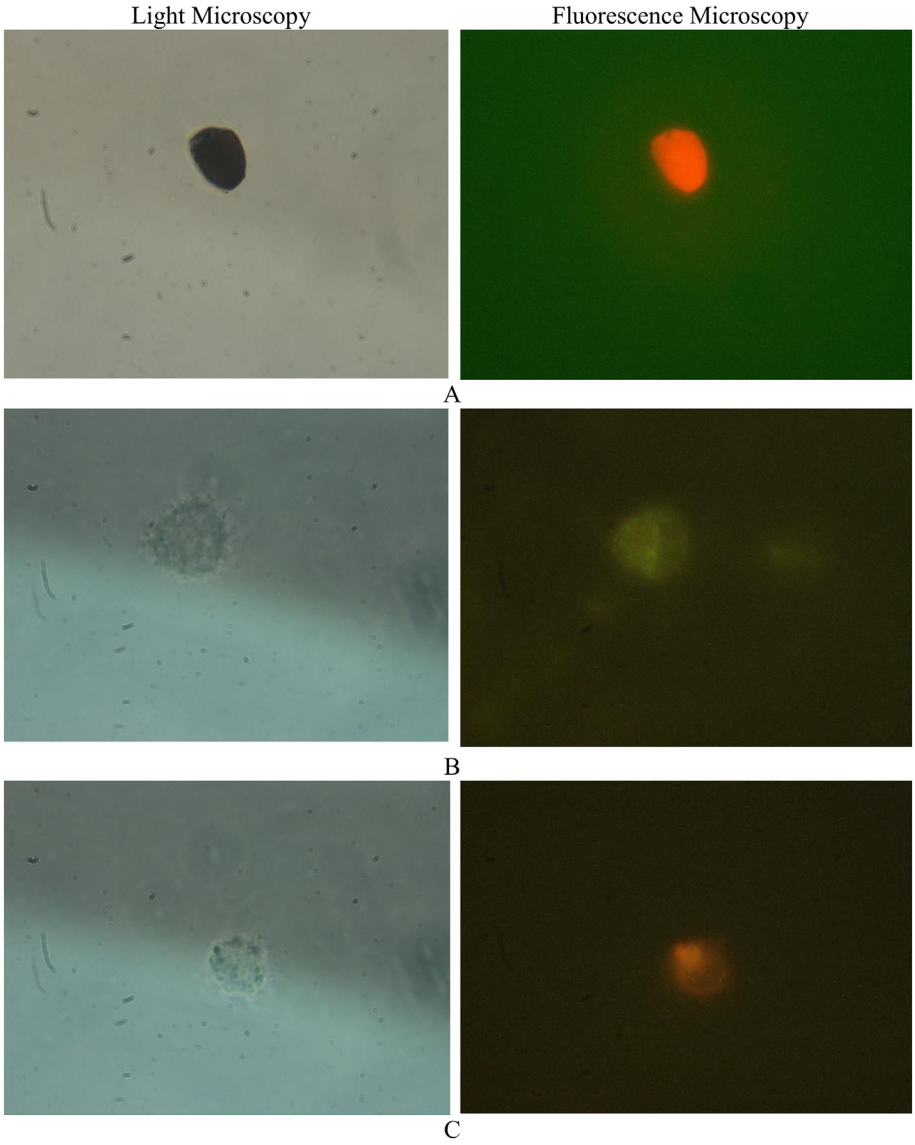

Fig. 10. Fluorescence photomicrography of a cluster of TiO_2 NPs loaded with hypericin (A). HuMDM cells were incubated in the presence of loaded NPs for 2 h (B) or 4 h (C).

antileishmania behavior. These phenomena have already been widely observed in the antimicrobial response of several semiconductor structures which principle of action is the production of ROS [61]. Additionally, NPs cytotoxicity for host cells was evaluated under darkness and visible irradiation for 40 min (Fig. 12B) and compared to anti-leishmanial activities to determine selectivity index (SI) which is the ratio between CC50 for macrophages and EC50 for the parasite (Table 2). The higher the SI, the more selective the compound is for the parasite. TiO_2 compounds doped with Fe and Pt did not present cytotoxicity under dark conditions, except for TiO_2 doped with Zn, which presented a CC_{50} concentration of 44.9 ± 6.7 μg/mL. It is important to note that Zn has been reported as an antimicrobial material due to its ability to generate hydrogen peroxide or electrostatic binding to the cell surface [53]. When systems were subjected to visible irradiation, cytotoxicity increased significantly for compounds doped with Pt and Zn. Measured values were Pt- (CC_{50} = 58.3 ± 4.7 μg/mL, SI = 3.2) and Zn- (CC_{50} = 30.4 ± 3.5 μg/mL, SI = 1.9) respectively. Doped TiO_2 are three and two fold more selective to the parasite, respectively, in comparison to the other compounds. In addition to the direct ROS effect on parasite viability and considering that both Pt- and Zn- doped TiO_2 presented similar levels of ROS, which is in accordance with similar EC_{50} values obtained, Zn doped TiO_2 NP was slightly more cytotoxic to the host cells. This is probably due to the well-known antimicrobial activity and cytotoxicity of Zn dopant [62–66] [53]. Fig. 13 summarize the possible mechanism of action of light activated Pt- TiO2 and Zn- TiO2, i.e., might be related to ROS production, leading to lipid peroxidation of plasma membrane and damage to essential macromolecules, among others [67]. Thus, in order to get insight about the exact mechanism of action caused by the doped TiO_2 compounds, it is necessary to carry out additional studies, which are beyond the scope of this work.

4. Conclusions

TiO_2 compounds doped with Fe, Pt or Zn were successfully synthesized by combustion route in solution. The powders obtained consisted of aggregates of particles at nanometric size (< 100 nm). The doping shifted the absorption of compounds towards the visible region of the electromagnetic spectrum (red-shift), followed by increased levels of ROS for Zn- or Pt- TiO_2 doped compounds, which might be correlated to the observed antileishmanial activity. Indirect fluorescence analyses showed that TiO_2 compounds are inside the cells, suggesting their uptake by the cells herein used only 2 h after incubation. Visible- light induced antileishmanial activity of Zn- or Pt- TiO2 doped

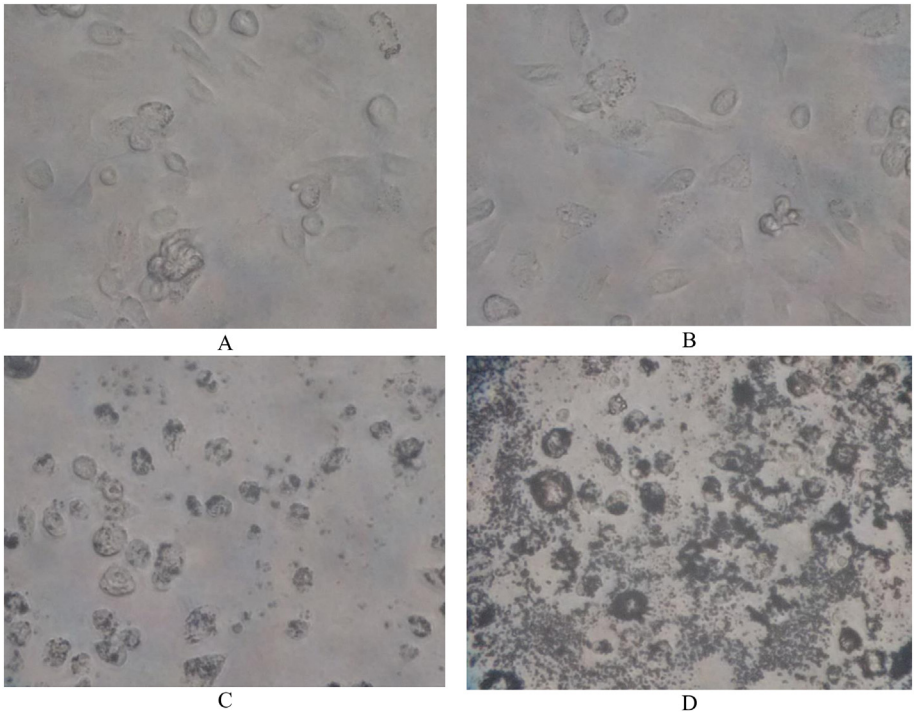

Fig. 11. Optical microscopy images. A–B) Macrophages control incubated 2 h without compounds. C) Macrophages incubated during 2 h with 10 μg/mL of Ti NPs. D) Macrophages incubated during 2 h with 20 μg/mL of Ti NPs.

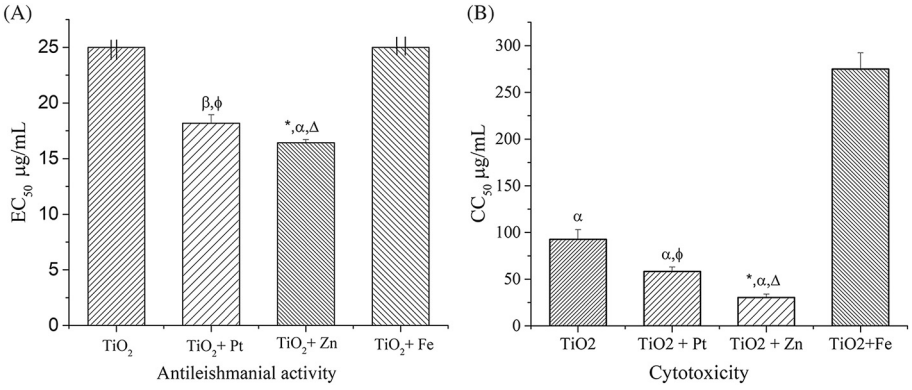

Fig. 12. In vitro effect of TiO_2 compounds with and without doping against mouse peritoneal macrophage at a light dose of 55 J/cm^2. A) Antileishmanial activities (EC50, half maximal inhibitory concentration). B) mammalian cell toxicity (CC50, half maximal cytotoxicity concentration). Results are expressed as mean ± standard deviation (SD). α: statistically significant difference with TiO_2 + Fe treatment ($p < 0.001$). *,ϕ: statistically significant difference with TiO_2 treatment ($p < 0.001$; $p < 0.01$). Δ: Statistically significant difference with TiO_2 + Pt treatment ($p < 0.05$).

Table 2
Antileishmanial activities (EC50, half maximal inhibitory concentration) and mammalian cell toxicity (CC50, half maximal cytotoxicity concentration) of TiO_2 NPs in the presence of light and their Selective Index (SI = CC50/EC50). Data are expressed as mean ± SD, $p < 0.05$.

Compound	EC_{50} (μg/mL) (light)	CC_{50} (μg/mL) (light)	CC_{50} (μg/mL) (darkness)	SI
TiO_2	NE	92.8 ± 10.3	NE	ND
TiO_2 + Pt	18.2 ± 0.8	58.3 ± 4.7	NE	3.2
TiO_2 + Zn	16.4 ± 0.3	30.4 ± 3.5	44.9 ± 6.7	1.9
TiO_2 + Fe	NE	275.1 ± 17.3	NC	ND

NE: Not effective; NC: Non Cytotoxic; ND: Not Determined.

compounds, which were also at least two-times more selective to the parasite than to the host cells. The antiparasitic activity observed for the Zn and Pt doped compounds might be attributed to ROS production, considering that TiO_2 and TiO_2Fe- doped compounds did not present neither leishmanicidal effect nor considerable ROS level. In summary, our results suggest that metal-doped TiO_2 might be a potential photo-activated compounds for treatment of CL through PDT.

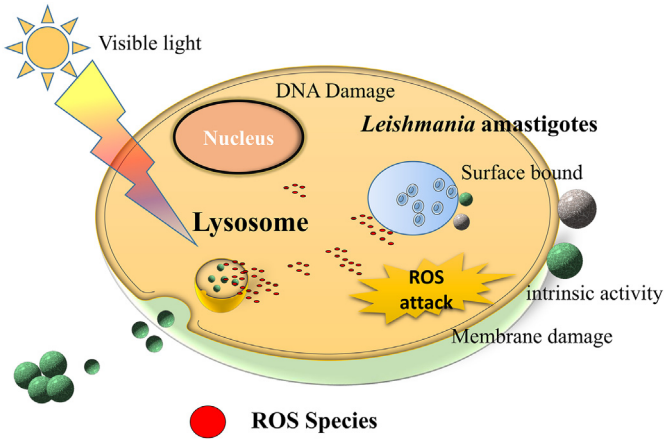

Fig. 13. Schematic mechanism of antileishmanial and citotoxicity effect of nanoparticles and their ions generate ROS, and induce oxidative stress resulting in the damage of DNA.

Acknowledgements

We thank the São Paulo Research Foundation (FAPESP) for financial support grants #2013/08248-1, #2016/05345-4 and #2017/03552-5 and Programa de Apoio ao Desenvolvimento Científico da Faculdade de Ciências Farmacêuticas da UNESP (PADC). AAL was supported by TWAS-CNPq Postgraduate Fellowship (Programme of Brazil, Colciencias, Proyecto "Doctorados Nacionales convocatoria 6172"; Universidad Nacional de Colombia, Medellín); AMAV and LMF were supported by FAPESP (#16/19289-9 and # 14/24581-5, respectively) and LCC supported by CAPES (Coordenação de Aperfeiçoamento de Pessoal de Nível Superior).

References

[1] Neglected tropical diseases, Available from: http://www.who.int/neglected_diseases/diseases/en/, .
[2] H.W. Murray, J.D. Berman, C.R. Davies, N.G. Saravia, Advances in leishmaniasis, Lancet 366 (9496) (2005) 1561–1577, http://dx.doi.org/10.1016/s0140-6736(05)67629-5 (PubMed PMID: WOS:000232984800026).
[3] WHO, Control of Leishmaniasis. Report of a Meeting of the WHO Expert Committee on the Control of Leishmaniasis. 22–26 March 2010, Geneva, World Health Organization, 2010.
[4] N. Singh, M. Kumar, R.K. Singh, Leishmaniasis: current status of available drugs and new potential drug targets, Asian Pac J Trop Med 5 (6) (2012) 485–497, http://dx.doi.org/10.1016/S1995-7645(12)60084-4 (PubMed PMID: 22575984).
[5] L.A. Dutra, L. de Almeida, T.G. Passalacqua, J.S. Reis, F.A.E. Torres, I. Martinez, et al., Leishmanicidal activities of novel synthetic furoxan and benzofuroxan derivatives, Antimicrob. Agents Chemother. 58 (8) (2014) 4837–4847, http://dx.doi.org/10.1128/aac.00052-14 (PubMed PMID: WOS:000339259200069).
[6] F.A.E. Torres, T.G. Passalacqua, A.M.A. Velasquez, R.A. de Souza, P. Colepicolo, M.A.S. Graminha, New drugs with antiprotozoal activity from marine algae: a review, Rev. Bras. Farm. 24 (3) (2014) 265–276, http://dx.doi.org/10.1016/j.bjp.2014.07.001 (PubMed PMID: WOS:000340839200001).
[7] T.G. Passalacqua, F.A.E. Torres, C.T. Nogueira, L. de Almeida, M.L. Del Cistia, M.B. dos Santos, et al., The 2′,4′-dihydroxychalcone could be explored to develop new inhibitors against the glycerol-3-phosphate dehydrogenase from Leishmania species, Bioorg. Med. Chem. Lett. 25 (17) (2015) 3564–3568, http://dx.doi.org/10.1016/j.bmcl.2015.06.085 (PubMed PMID: WOS:000358802900029).
[8] T.G. Passalacqua, L.A. Dutra, L. de Almeida, A.M. Arenas Velasquez, F.A. Esteves Torres, P.R. Yamasaki, et al., Synthesis and evaluation of novel prenylated chalcone derivatives as anti-leishmanial and anti-trypanosomal compounds, Bioorg. Med. Chem. Lett. 25 (16) (2015) 3342–3345, http://dx.doi.org/10.1016/j.bmcl.2015.05.072 (PubMed PMID: WOS:000357572000053).
[9] A. Velásquez, R. Souza, T. Passalacqua, A. Ribeiro, M. Scontri, C. Chin, et al., Antiprotozoal activity of the cyclopalladated complexes against Leishmania amazonensis and Trypanosoma cruzi, J. Braz. Chem. Soc. 27 (6) (2016) 1032–1039, http://dx.doi.org/10.5935/0103-5053.20150360 (Epub 12/21/2015).
[10] V.A.F.F.M. Santos, L.O. Regasini, C.R. Nogueira, G.D. Passerini, I. Martinez, V.S. Bolzani, et al., Antiprotozoal sesquiterpene pyridine alkaloids from Maytenus ilicifolia, J. Nat. Prod. 75 (5) (2012) 991–995, http://dx.doi.org/10.1021/np300077r (PubMed PMID: WOS:000304385800021).
[11] V.A.F.F.M. dos Santos, K.M. Leite, MdC Siqueira, L.O. Regasini, I. Martinez, C.T. Nogueira, et al., Antiprotozoal activity of quinonemethide triterpenes from Maytenus ilicifolia (Celastraceae), Molecules 18 (1) (2013) 1053–1062, http://dx.doi.org/10.3390/molecules18011053 (PubMed PMID: WOS:000314032900065).
[12] A. Coqueiro, L.O. Regasini, G.M. Leme, L. Polese, C.T. Nogueira, M.L. Del Cistia, et al., Leishmanicidal activity of Brosimum glaziovii (Moraceae) and chemical composition of the bioactive fractions by using high-resolution gas chromatography and GC-MS, J. Braz. Chem. Soc. 25 (10) (2014) 1839, http://dx.doi.org/10.5935/0103-5053.20140138 (PubMed PMID: WOS:000344490900009).
[13] A.V. Silva, A. López-Sánchez, H.C. Junqueira, L. Rivas, M.S. Baptista, G. Orellana, Riboflavin derivatives for enhanced photodynamic activity against Leishmania parasites, Tetrahedron 71 (3) (2015) 457–462, http://dx.doi.org/10.1016/j.tet.2014.11.072.
[14] L.S. Peloi, C.E. Biondo, E. Kimura, M.J. Politi, M.V. Lonardoni, S.M. Aristides, et al., Photodynamic therapy for American cutaneous leishmaniasis: the efficacy of methylene blue in hamsters experimentally infected with Leishmania (Leishmania) amazonensis, Exp. Parasitol. 128 (4) (2011) 353–356, http://dx.doi.org/10.1016/j.exppara.2011.04.009 (PubMed PMID: 21575635).
[15] O.E. Akilov, S. Kosaka, K. O'Riordan, T. Hasan, Photodynamic therapy for cutaneous leishmaniasis: the effectiveness of topical phenothiaziniums in parasite eradication and Th1 immune response stimulation, Photochem. Photobiol. Sci. 6 (10) (2007) 1067–1075.
[16] K.P. Chang, B.K. Kolli, New "light" for one-world approach toward safe and effective control of animal diseases and insect vectors from leishmaniac perspectives, Parasit. Vectors 9 (1) (2016) 396.
[17] M.S. Baptista, M. Wainwright, Photodynamic antimicrobial chemotherapy (PACT) for the treatment of malaria, leishmaniasis and trypanosomiasis, Braz. J. Med. Biol. Res. 44 (1) (2011) 1–10, http://dx.doi.org/10.1590/s0100-879x2010007500141 (PubMed PMID: WOS:000286321100001).
[18] J. Montanari, C. Maidana, M.I. Esteva, C. Salomon, M.J. Morilla, E.L. Romero, Sunlight triggered photodynamic ultradeformable liposomes against Leishmania braziliensis are also leishmanicidal in the dark, J. Control. Release 147 (3) (2010) 368–376.
[19] D. Song, J.A.L. Lindoso, L.K. Oyafuso, E.H.Y. Kanashiro, J.L. Cardoso, A.F. Uchoa, et al., Photodynamic therapy using methylene blue to treat cutaneous leishmaniasis, Photomed. Laser Surg. 29 (10) (2011) 711–715.
[20] L.S. Peloi, C.E.G. Biondo, E. Kimura, M.J. Politi, M.V.C. Lonardoni, S.M.A. Aristides, et al., Photodynamic therapy for American cutaneous leishmaniasis: the efficacy of methylene blue in hamsters experimentally infected with Leishmania (Leishmania) amazonensis, Exp. Parasitol. 128 (4) (2011) 353–356.
[21] P. Escobar, I.P. Hernández, C.M. Rueda, F. Martínez, E. Páez, Photodynamic activity of aluminium (III) and zinc (II) phthalocyanines in Leishmania promastigotes, Biomedica 26 (2006) 49–56.
[22] R. Yin, T. Dai, P. Avci, A.E.S. Jorge, W.C. de Melo, D. Vecchio, et al., Light based anti-infectives: ultraviolet C irradiation, photodynamic therapy, blue light, and beyond, Curr. Opin. Pharmacol. 13 (5) (2013) 731–762.
[23] B. Bethi, S.H. Sonawane, B.A. Bhanvase, S.P. Gumfekar, Nanomaterials-based advanced oxidation processes for wastewater treatment: a review, Chem. Eng. Process. 109 (Suppl. C) (2016) 178–189, http://dx.doi.org/10.1016/j.cep.2016.08.016.
[24] N. Shaham-Waldmann, Y. Paz, Away from TiO_2: a critical minireview on the developing of new photocatalysts for degradation of contaminants in water, Mater. Sci. Semicond. Process. 42 (Part 1) (2016) 72–80, http://dx.doi.org/10.1016/j.mssp.2015.06.068.
[25] A.M. Allahverdiyev, E.S. Abamor, M. Bagirova, S.Y. Baydar, S.C. Ates, F. Kaya, et al., Investigation of antileishmanial activities of Tio2@Ag nanoparticles on biological properties of L. tropica and L. infantum parasites, in vitro, Exp. Parasitol. 135 (1) (2013) 55–63, http://dx.doi.org/10.1016/j.exppara.2013.06.001.
[26] A. Jebali, B. Kazemi, Nano-based antileishmanial agents: a toxicological study on nanoparticles for future treatment of cutaneous leishmaniasis, Toxicol. in Vitro 27 (6) (2013) 1896–1904, http://dx.doi.org/10.1016/j.tiv.2013.06.002.
[27] E.S. Abamor, A.M. Allahverdiyev, A nanotechnology based new approach for chemotherapy of cutaneous Leishmaniasis: TIO2@AG nanoparticles – Nigella sativa oil combinations, Exp. Parasitol. 166 (2016) 150–163, http://dx.doi.org/10.1016/j.exppara.2016.04.008.
[28] E.S. Abamor, A.M. Allahverdiyev, M. Bagirova, M. Rafailovich, Meglumine antımoniate-TiO2@Ag nanoparticle combinations reduce toxicity of the drug while enhancing its antileishmanial effect, Acta Trop. 169 (2017) 30–42, http://dx.doi.org/10.1016/j.actatropica.2017.01.005.
[29] A.M. Allahverdiyev, E.S. Abamor, M. Bagirova, C.B. Ustundag, C. Kaya, F. Kaya, et al., Antileishmanial effect of silver nanoparticles and their enhanced antiparasitic activity under ultraviolet light, Int. J. Nanomedicine 6 (2011) 2705–2714.
[30] C.A. Rebeiz, L.J. Guta, K. Leea, J.A. Juvika, C.C. Rebeiza, C.E. Boutona, Photodynamics of porphyric insecticides, Crit. Rev. Plant Sci. 14 (1995), http://dx.doi.org/10.1080/07352689509382363.
[31] A. Lopera, E. Chavarriaga, H. Estupiñan, I. Valencia, C. Paucar, C. Garcia, Synthesis and spectroscopic characterization of nanoparticles of TiO_2 doped with Pt produced via the self-combustion route, J. Phys. D. Appl. Phys. 49 (20) (2016) 205501.
[32] X. Ma, L. Xue, X. Li, M. Yang, Y. Yan, Controlling the crystalline phase of TiO_2 powders obtained by the solution combustion method and their photocatalysis activity, Ceram. Int. 41(9 (2015) 11927–11935.
[33] M. Sadat-Shojai, M.T. Khorasani, E. Dinpanah-Khoshdargi, A. Jamshidi, Synthesis methods for nanosized hydroxyapatite with diverse structures, Acta Biomater. 9 (8) (2013) 7591–7621, http://dx.doi.org/10.1016/j.actbio.2013.04.012 (PubMed PMID: 23583646).
[34] H. Rietveld, A profile refinement method for nuclear and magnetic structures, J. Appl. Crystallogr. 2 (2) (1969) 65–71.
[35] A. Larson, R. Von Dreele, Gsas: General Structure Analysis System Report LAUR 86–748, Los Alamos National Laboratory, Los Alamos, NM, 1986.
[36] A. Velásquez, Souza RAD, T.G. Passalacqua, A.R. Ribeiro, M. Scontri, C.M. Chin, et al., Antiprotozoal activity of the cyclopalladated complexes against Leishmania amazonensis and Trypanosoma cruzi, J. Braz. Chem. Soc. 27 (6) (2016) 1032–1039.
[37] A. Montoya, A. Daza, D. Muñoz, K. Ríos, V. Taylor, D. Cedeño, et al., Development of a novel formulation with hypericin to treat cutaneous leishmaniasis based on photodynamic therapy in in vitro and in vivo studies, Antimicrob. Agents Chemother. 59 (9) (2015) 5804–5813.
[38] K. Tomankova, J. Horakova, M. Harvanova, L. Malina, J. Soukupova, S. Hradilova, et al., Cytotoxicity, cell uptake and microscopic analysis of titanium dioxide and silver nanoparticles in vitro, Food Chem. Toxicol. 82 (2015) 106–115, http://dx.doi.org/10.1016/j.fct.2015.03.027 (PubMed PMID: 25846500).
[39] C.F. Macrae, P.R. Edgington, P. McCabe, E. Pidcock, G.P. Shields, R. Taylor, et al., Mercury: visualization and analysis of crystal structures, J. Appl. Crystallogr. 39 (3) (2006) 453–457.
[40] F.H. Allen, The Cambridge structural database: a quarter of a million crystal structures and rising, Acta Crystallogr. Sect. B: Struct. Sci. 58 (3) (2002) 380–388.
[41] W.Y. Teoh, L. Mädler, D. Beydoun, S.E. Pratsinis, R. Amal, Direct (one-step) synthesis of TiO2 and Pt/TiO2 nanoparticles for photocatalytic mineralisation of sucrose, Chem. Eng. Sci. 60 (21) (2005) 5852–5861, http://dx.doi.org/10.1016/j.ces.2005.05.037.
[42] K. Kaviyarasu, N. Geetha, K. Kanimozhi, C. Maria Magdalane, S. Sivaranjani, A. Ayeshamariam, et al., In vitro cytotoxicity effect and antibacterial performance of human lung epithelial cells A549 activity of zinc oxide doped TiO2 nanocrystals: investigation of bio-medical application by chemical method, Mater. Sci. Eng. C 74 (2017) 325–333, http://dx.doi.org/10.1016/j.msec.2016.12.024.
[43] C.Y.W. Lin, D. Channei, P. Koshy, A. Nakaruk, C.C. Sorrell, Effect of Fe doping on TiO2 films prepared by spin coating, Ceram. Int. 38 (5) (2012) 3943–3946, http://

dx.doi.org/10.1016/j.ceramint.2012.01.047.
[44] M. Sanchez-Dominguez, G. Morales-Mendoza, M.J. Rodriguez-Vargas, C.C. Ibarra-Malo, A.A. Rodriguez-Rodriguez, A.V. Vela-Gonzalez, et al., Synthesis of Zn-doped TiO2 nanoparticles by the novel oil-in-water (O/W) microemulsion method and their use for the photocatalytic degradation of phenol, J. Environ. Chem. Eng. 3 (4, Part B) (2015) 3037–3047, http://dx.doi.org/10.1016/j.jece.2015.03.010.
[45] H. Moradi, A. Eshaghi, S.R. Hosseini, K. Ghani, Fabrication of Fe-doped TiO2 nanoparticles and investigation of photocatalytic decolorization of reactive red 198 under visible light irradiation, Ultrason. Sonochem. 32 (2016) 314–319, http://dx.doi.org/10.1016/j.ultsonch.2016.03.025.
[46] Y. Hu, X. Song, S. Jiang, C. Wei, Enhanced photocatalytic activity of Pt-doped TiO2 for NOx oxidation both under UV and visible light irradiation: a synergistic effect of lattice Pt4+ and surface PtO, Chem. Eng. J. 274 (2015) 102–112, http://dx.doi.org/10.1016/j.cej.2015.03.135.
[47] R.G. Nair, S. Mazumdar, B. Modak, R. Bapat, P. Ayyub, K. Bhattacharyya, The role of surface O-vacancies in the photocatalytic oxidation of Methylene Blue by Zn-doped TiO2: a mechanistic approach, J. Photochem. Photobiol. A Chem. 345 (2017) 36–53, http://dx.doi.org/10.1016/j.jphotochem.2017.05.016.
[48] A.G. Ilie, M. Scarisoareanu, I. Morjan, E. Dutu, M. Badiceanu, I. Mihailescu, Principal component analysis of Raman spectra for TiO2 nanoparticle characterization, Appl. Surf. Sci. 417 (2017) 93–103, http://dx.doi.org/10.1016/j.apsusc.2017.01.193.
[49] K. Patil, Chemistry of Nanocrystalline Oxide Materials: Combustion Synthesis, Properties and Applications, World Scientific, 2008.
[50] D. Sethi, R. Sakthivel, ZnO/TiO2 composites for photocatalytic inactivation of Escherichia coli, J. Photochem. Photobiol. B Biol. 168 (2017) 117–123, http://dx.doi.org/10.1016/j.jphotobiol.2017.02.005.
[51] Ö. Kerkez-Kuyumcu, E. Kibar, K. Dayıoğlu, F. Gedik, A.N. Akın, Ş. Özkara-Aydınoğlu, A comparative study for removal of different dyes over M/TiO2 (M = Cu, Ni, Co, Fe, Mn and Cr) photocatalysts under visible light irradiation, J. Photochem. Photobiol. A Chem. 311 (2015) 176–185, http://dx.doi.org/10.1016/j.jphotochem.2015.05.037.
[52] J. Wang, Y.F. Zhao, T. Wang, H. Li, C. Li, Photonic, and photocatalytic behavior of TiO2 mediated by Fe, CO, Ni, N doping and co-doping, Phys. B Condens. Matter 478 (2015) 6–11, http://dx.doi.org/10.1016/j.physb.2015.08.020.
[53] K. Vijayalakshmi, A. Renitta, K. Karthick, Growth of high quality ZnO:Mg films on ITO coated glass substrates for enhanced H2 sensing, Ceram. Int. 40 (4) (2014) 6171–6177, http://dx.doi.org/10.1016/j.ceramint.2013.11.070.
[54] R. Sanjines, H. Tang, H. Berger, F. Gozzo, G. Margaritondo, F. Levy, Electronic structure of anatase TiO2 oxide, J. Appl. Phys. 75 (6) (1994) 2945–2951.
[55] K.C. Patil, S.T. Aruna, T. Mimani, Combustion synthesis: an update, Curr. Opinion Solid State Mater. Sci. 6 (6) (2002) 507–512.
[56] S.M. AL-Jawad, A.A. Taha, M.M. Salim, Synthesis and characterization of pure and Fe doped TiO2 thin films for antimicrobial activity, Int. J. Light Electron Optics 142 (2017) 42–53.
[57] J. Schwiertz, A. Wiehe, S. Grafe, B. Gitter, M. Epple, Calcium phosphate nanoparticles as efficient carriers for photodynamic therapy against cells and bacteria, Biomaterials 30 (19) (2009) 3324–3331, http://dx.doi.org/10.1016/j.biomaterials.2009.02.029 (PubMed PMID: 19304318).
[58] V. Sokolova, D. Kozlova, T. Knuschke, J. Buer, A.M. Westendorf, M. Epple, Mechanism of the uptake of cationic and anionic calcium phosphate nanoparticles by cells, Acta Biomater. 9 (7) (2013) 7527–7535, http://dx.doi.org/10.1016/j.actbio.2013.02.034 (PubMed PMID: 23454056).
[59] Z.E. Allouni, P.J. Hol, M.A. Cauqui, N.R. Gjerdet, M.R. Cimpan, Role of physicochemical characteristics in the uptake of TiO_2 nanoparticles by fibroblasts, Toxicol. in Vitro 26 (3) (2012) 469–479, http://dx.doi.org/10.1016/j.tiv.2012.01.019 (PubMed PMID: 22300586).
[60] S. Picchietti, C. Bernini, V. Stocchi, A.R. Taddei, R. Meschini, A.M. Fausto, et al., Engineered nanoparticles of titanium dioxide (TIO2): uptake and biological effects in a sea bass cell line, Fish Shellfish Immunol. 63 (2017) 53–67, http://dx.doi.org/10.1016/j.fsi.2017.01.044 (PubMed PMID: 28159697).
[61] P.I. Rajan, J.J. Vijaya, S.K. Jesudoss, K. Kaviyarasu, L.J. Kennedy, R. Jothiramalingam, et al., Green-fuel-mediated synthesis of self-assembled NiO nano-sticks for dual applications—photocatalytic activity on Rose Bengal dye and antimicrobial action on bacterial strains, Mat. Res. Express 4 (8) (2017) 085030.
[62] J. Borovanský, P.A. Riley, Cytotoxicity of zinc in vitro, Chem. Biol. Interact. 69 (2–3) (1989) 279–291.
[63] J. Borovansky, M. Blasko, J. Siracky, A. Schothorst, N. Smit, S. Pavel, Cytotoxic interactions of Zn2+ in vitro: melanoma cells are more susceptible than melanocytes, Melanoma Res. 7 (6) (1997) 449–453.
[64] J. Wu, L. Wang, J. He, C. Zhu, In vitro cytotoxicity of Cu2+, Zn2+, Ag+ and their mixtures on primary human endometrial epithelial cells, Contraception 85 (5) (2012) 509–518, http://dx.doi.org/10.1016/j.contraception.2011.09.016.
[65] J. Ma, A. Hui, J. Liu, Y. Bao, Controllable synthesis of highly efficient antimicrobial agent-Fe doped sea urchin-like ZnO nanoparticles, Mater. Lett. 158 (Suppl. C) (2015) 420–423, http://dx.doi.org/10.1016/j.matlet.2015.06.037.
[66] K. Kaviyarasu, C. Maria Magdalane, K. Kanimozhi, J. Kennedy, B. Siddhardha, E. Subba Reddy, et al., Elucidation of photocatalysis, photoluminescence and antibacterial studies of ZnO thin films by spin coating method, J. Photochem. Photobiol. B Biol. 173 (2017) 466–475, http://dx.doi.org/10.1016/j.jphotobiol.2017.06.026.
[67] A.A. Ezhilarasi, J.J. Vijaya, K. Kaviyarasu, M. Maaza, A. Ayeshamariam, L.J. Kennedy, Green synthesis of NiO nanoparticles using Moringa oleifera extract and their biomedical applications: cytotoxicity effect of nanoparticles against HT-29 cancer cells, J. Photochem. Photobiol. B Biol. 164 (2016) 352–360, http://dx.doi.org/10.1016/j.jphotobiol.2016.10.003.